

The DFT+ Σ_2 method for electron correlation effects at transition metal surfaces

Andrea Droghetti^{‡,1,*} Miloš M. Radonjić^{‡,2} Anita Halder,¹ Ivan Rungger,³ and Liviu Chioncel⁴

¹*School of Physics and CRANN, Trinity College, Dublin 2, Ireland*

²*Institute of Physics Belgrade, University of Belgrade, Pregrevica 118, 11080 Belgrade, Serbia*

³*National Physical Laboratory, Hampton Road, Teddington TW11 0LW, United Kingdom*

⁴*Theoretical Physics III, Center for Electronic Correlations and Magnetism, Institute of Physics, and Augsburg Center for Innovative Technologies, University of Augsburg, 86135 Augsburg, Germany*

We present a computational approach for electronically correlated metallic surfaces and interfaces, which combines Density Functional and Dynamical Mean Field Theory using a multi-orbital perturbative solver for the many-body problem. The performances are assessed in detail for a Fe monolayer on a W(110) substrate, a prototypical nanoscale magnetic system. We find qualitative and quantitative improvements in the calculated spectral function compared to the results of density functional theory within the local spin density approximation. In particular, the spin-splitting of the d states is drastically reduced and, at the same time, their spectral width becomes narrower. Additionally, the method predicts the appearance of satellites, genuine many-body effects, at higher binding energies.

I. INTRODUCTION

Metallic heterostructures, formed by stacking different thin films, are the building blocks of spintronic devices, such as spin-valves. Their functionalities are largely determined by the interfaces between the various layers and by the presence of ferromagnetic transition metals (TMs), such as Fe, Co and Ni. Owing to their partially filled $3d$ shells, the electronic structure of these compounds is characterized by electron correlations, which are modified and possibly enhanced at surfaces and interfaces because of atomic relaxation and, moreover, of the reduced atomic coordination. These effects can now be studied in very great detail thanks to the dramatic advancement of spectroscopic¹ and scanning probe techniques². Yet a proper understanding and interpretation of the data requires accurate *ab-initio* simulations. Density Functional Theory (DFT)^{3–5} with its various formulations for the exchange-correlation functionals such as the local spin density approximation (LSDA)^{6,7} or the generalized gradient approximation (GGA)^{8–10} provides a reasonable description for many of the ground state properties of bulk $3d$ transition metals, but turns out insufficient for describing the excitation spectra of Fe, Ni and Co as measured in photoemission spectroscopy^{11,12}. The DFT band structure drastically overestimates the spin splitting of the $3d$ bands and gives too wide majority spin bands. Furthermore, DFT does not capture intrinsic many-electron spectroscopic features, such as satellites¹³. Electronic correlations can be described within the Hubbard model, which has been extended and combined with DFT to incorporate the realistic description of materials¹⁴. In the so-called DFT+U method^{15–18}, an effective Hubbard-like interaction is added to the LSDA/GGA exchange-correlation density functional and treated at

the static mean-field level. The method has found widespread use for computational materials design. However, when applied to Fe, Ni and Co, it gives a rigid downward shift of the majority spin bands, while the minority states are maintained at the same positions. As a result, the spin-splitting of the bands is even more overestimated than in LSDA/GGA calculations¹⁸, while majority spin $3d$ bands remain too wide. Hence, the U static potential actually worsen, instead of improving, the accuracy of DFT for these systems.

During the last decade, much progress in the theoretical understanding of $3d$ TMs beyond the limitations of the static mean-field DFT+U picture have been achieved through dynamical mean-field theory (DMFT)^{19–22}. In the so-called LSDA+DMFT scheme^{22,23}, LSDA calculations provide the *ab-initio* material dependent inputs (orbitals and hopping parameters), while DMFT solves the many-body problem for the local interactions. LSDA+DMFT has been applied to address spectral properties of $3d$ ferromagnetic TMs bulk^{24,25} and surfaces²⁵, TM alloys²⁶ and TM compounds²⁷, and to estimate magnetic moments above and below the Curie temperature²⁴. Electronic correlation effects have been also investigated in digital magnetic heterostructures^{28,29} or interfaces containing half-metallic ferromagnets^{30,31}. Tunable interfacial properties, which emerge in the presence of electronic correlation, have been found in ferromagnetic heterostructures³². Last but not least, surface properties have been studied^{25,30,31} in connection to linear-response spin-dependent charge transport^{33,34}.

Despite all these successes, in practice LSDA+DMFT remains a quite complex and a computationally demanding approach especially for inhomogeneous systems like heterostructures and interfaces. Furthermore, the DMFT solvers^{35–38} typically used for ferromagnetic metals are formulated on the imaginary frequency axis and spectral functions are obtained using numerical analytic continuation schemes to the real frequency axis^{39–41}. The resulting spectra are noisy and sharp features are absent

[‡]These authors contributed equally to this work.

or smeared out. This leads to difficulties when comparing theoretical results to spectroscopic data and when computing spin-transport properties via generalized Landauer approaches^{42,43}, which require the integration of the frequency-dependent transmission function^{33,44}. Hence, DMFT solvers that capture the essential correlation features at a lower computational cost and that are easily implemented using real instead of imaginary frequencies are very valuable.

In this paper, we present one of such methods. In particular, we show that the many-electron physics at 3d TM surfaces can be treated perturbatively up to the second order in the local Coulomb interaction parameter U , while keeping the full manifold of all correlated orbitals provided within DFT. We name this method DFT+ Σ_2 as second order contributions are calculated diagrammatically on the real frequency axis and accounted for via a self-energy Σ_2 . While the Σ_2 self-energy has been evaluated in a number of studies about model systems^{45,46}, we are not aware of any previous paper, where it has been systematically combined with DFT and used for describing interfaces and heterostructures. The results of DFT+ Σ_2 are generally accurate for moderately correlated systems, such as 3d TMs, where U is smaller or comparable to the band width. According to the Fermi-liquid theory the net results of a Σ_2 self-energy is that the spin-splitting of the correlated states is drastically reduced and, at the same time, their spectral width becomes narrower compared to LSDA calculations. As a specific example, we study a Fe mono-layer on a W(110) substrate, a prototypical ultra-thin magnetic film extensively studied experimentally, and which is used, for example, in tunneling magnetoresistance measurements^{47,48}. We find a drastic improvement of the spectral function of the 3d Fe orbitals compared to the results of DFT and DFT+ U . Moreover, we predict the appearance of satellite features at high energies below the Fermi level.

The paper is organized as follows. To begin with, we present the method and the details of our numerical implementation in Sections II and III. A complete derivation of the Σ_2 self-energy is presented in the Appendix. In section IV, we then show the results for Fe on W(110) comparing the density of states calculated with DFT, DFT+ U and DFT+ Σ_2 . Finally we conclude highlighting the strengths of the method and anticipating potential future applications.

II. METHOD AND IMPLEMENTATION

We employ the electronic structure code Smeagol^{44,49}, which implements DFT through the Green's function formalism. Smeagol uses a linear combination of atomic orbitals (LCAO) basis set according to a multiple-zetas scheme⁵⁰ and obtains the LSDA KS Hamiltonian from the DFT package Siesta⁵¹. However, the equations presented in the following are general and can be readily im-

plemented in any other DFT code based on the LCAO approach.

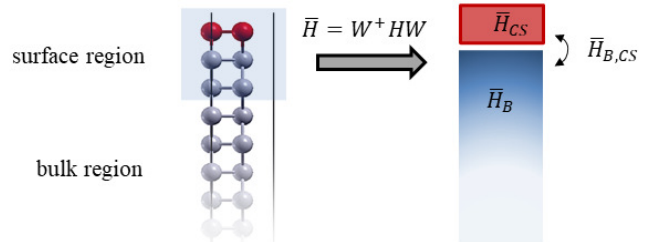


FIG. 1: One mono-layer of Fe on the W(110). The red and green spheres are respectively the Fe and W atoms. The surface region is contained in the light blue rectangle. The transformation, Eq. (3), which projects the correlated subspace Hamiltonian out of the surface region Hamiltonian is also shown schematically on the right-hand side.

A. System set-up and correlated subspace

The typical system that we study is shown in Fig. 1. It consists of few ferromagnetic TM layers on a semi-infinite non-magnetic substrate, where electron correlations are negligible. The surface is parallel to the x - y plane, while its normal vector points along the z direction. Periodic boundary conditions are applied along x and y so that $\mathbf{k} = (k_x, k_y)$ is the in-plane momentum. In practice the system is partitioned into the surface region (SR) and the bulk region. The surface region comprises not only the ferromagnetic layers, but also several layers underneath, as their electronic structure is different from that of the bulk layers. We denote the number of basis orbitals within the SR by N_{SR} . The (effectively) non-interacting LSDA KS Hamiltonian matrix of the SR for a given \mathbf{k} is $H^\sigma(\mathbf{k})$, where $\sigma = \uparrow, \downarrow$ labels the spin. Since in general the basis set is non-orthogonal, we also introduce the $N_{\text{SR}} \times N_{\text{SR}}$ orbital overlap matrix $S(\mathbf{k})$. The non-interacting frequency-dependent retarded Green's functions of the SR is then given in the standard form^{44,49}

$$\mathcal{G}^\sigma(\mathbf{k}, \omega) = [(\omega + i\eta)S(\mathbf{k}) - H^\sigma(\mathbf{k}) - \Delta^\sigma(\mathbf{k}, \omega)]^{-1} \quad (1)$$

which has a matrix structure analogous to the one of $H^\sigma(\mathbf{k})$ and $S(\mathbf{k})$; η is a vanishing small positive real number. The frequency-dependent and momentum-dependent embedding potential matrix $\Delta^\sigma(\mathbf{k}, \omega)$ accounts for the coupling between the SR and the bulk region and it is calculated by using the algorithm in Ref.⁵². Assuming that there are in total N_{TM} ferromagnetic TMs in the SR (see Fig. 1), their 3d orbitals span a $2(5 \times N_{\text{TM}})$ -dimensional subspace, that we call the ‘‘correlated subspace’’ (CS) (the factor 2 accounts for the spin).

The CS can be projected out from the rest of the system, which we refer to as the ‘‘bath’’ (B)^{42,43,53–55} and which includes the orthogonal subspace to the CS within the SR as well as the bulk region. In practice we use the algorithm in Ref.⁴³ and perform the transformations

$$\begin{aligned}\bar{S}(\mathbf{k}) &= \begin{pmatrix} 1 & 0 \\ 0 & \bar{S}_B(\mathbf{k}) \end{pmatrix} = \\ &= W(\mathbf{k})^\dagger S(\mathbf{k}) W(\mathbf{k})\end{aligned}\quad (2)$$

$$\begin{aligned}\bar{H}^\sigma(\mathbf{k}) &= \begin{pmatrix} \bar{H}_{CS}^\sigma(\mathbf{k}) & \bar{H}_{CS,B}^\sigma(\mathbf{k}) \\ \bar{H}_{B,CS}^\sigma(\mathbf{k}) & \bar{H}_B^\sigma(\mathbf{k}) \end{pmatrix} = \\ &= W(\mathbf{k})^\dagger H^\sigma(\mathbf{k}) W(\mathbf{k})\end{aligned}\quad (3)$$

$$\begin{aligned}\bar{\mathcal{G}}^\sigma(\mathbf{k}, \omega) &= \begin{pmatrix} \bar{\mathcal{G}}_{CS}^\sigma(\mathbf{k}, \omega) & \bar{\mathcal{G}}_{CS,B}^\sigma(\mathbf{k}, \omega) \\ \bar{\mathcal{G}}_{B,CS}^\sigma(\mathbf{k}, \omega) & \bar{\mathcal{G}}_B^\sigma(\mathbf{k}, \omega) \end{pmatrix} = \\ &= W(\mathbf{k})^{-1} \mathcal{G}^\sigma(\mathbf{k}, \omega) W(\mathbf{k})^{-1\dagger}\end{aligned}\quad (4)$$

bringing $S(\mathbf{k})$, $H^\sigma(\mathbf{k})$ and $\mathcal{G}^\sigma(\mathbf{k}, \omega)$ into their transformed $\bar{S}(\mathbf{k})$, $\bar{H}^\sigma(\mathbf{k})$ and $\bar{\mathcal{G}}^\sigma(\mathbf{k}, \omega)$, where the top left block describes the CS, the bottom right block describes the part of the bath included in the SR, and the off-diagonal blocks describe the connection terms. The matrices $W(\mathbf{k})$ are defined in Eq. (10) of Ref.⁴³. We note from Eq. (2) that the orbitals of the CS become orthogonal and they have zero overlap with the bath orbitals. $\bar{H}_{CS}^\sigma(\mathbf{k})$ in Eq. (3) and $\bar{\mathcal{G}}_{CS}^\sigma(\mathbf{k}, \omega)$ in Eq. (4) are respectively the non-interacting CS Hamiltonian and the non-interacting, or bare, CS retarded Green’s function matrices of dimension $5N_{\text{TM}} \times 5N_{\text{TM}}$.

In the second quantization formalism the CS Hamiltonian reads

$$\hat{H}_{CS}^\sigma(\mathbf{k}) = \sum_{i,j,\lambda_1,\lambda_2,\sigma} [\bar{H}_{CS}^\sigma(\mathbf{k})]_{i\lambda_1,j\lambda_2} \hat{d}_{i\lambda_1\sigma}^\dagger \hat{d}_{j\lambda_2\sigma} \quad (5)$$

where $\hat{d}_{i\lambda\sigma}^\dagger$ and $\hat{d}_{i\lambda\sigma}$ are the electron creation and annihilation operators at orbital λ within the atom i and spin σ ($i = 1, \dots, N_{\text{TM}}$ and $\lambda = 1, \dots, 5$, $\sigma = \uparrow, \downarrow$). $[\bar{H}_{CS}^\sigma(\mathbf{k})]_{i\lambda_1,j\lambda_2}$ is the CS Hamiltonian matrix element between the d orbital λ_1 of the atom i and the d orbital λ_2 of the atom j . The Hubbard-like electron-electron interaction term is added to \hat{H} as follow

$$\begin{aligned}\hat{H}^\sigma(\mathbf{k})_{CS,U} &= \hat{H}_{CS}^\sigma(\mathbf{k}) + \\ &+ \frac{1}{2} \sum_{\substack{i,\lambda_1,\lambda_2,\lambda_3, \\ \lambda_4,\sigma_1,\sigma_2}} U_{\lambda_1,\lambda_2,\lambda_3,\lambda_4} d_{i\lambda_1\sigma_1}^\dagger d_{i\lambda_2\sigma_2}^\dagger d_{i\lambda_4\sigma_2} d_{i\lambda_3\sigma_1} - \hat{H}_{CS,d}^\sigma\end{aligned}\quad (6)$$

where $U_{\lambda_1,\lambda_2,\lambda_3,\lambda_4}$ are the four-index U parameters, i.e. the matrix elements of the screened Coulomb interaction between four $3d$ orbitals located at the same site. They are parameterized in terms of the average effective Coulomb interaction U and exchange J ⁵⁶

$$U = \frac{1}{(2l+1)^2} \sum_{\lambda_1,\lambda_2} U_{\lambda_1,\lambda_2,\lambda_1,\lambda_2} \quad (7)$$

$$J = \frac{1}{2l(2l+1)} \sum_{\lambda_1 \neq \lambda_2,\lambda_2} U_{\lambda_1,\lambda_2,\lambda_2,\lambda_1}. \quad (8)$$

$\hat{H}_{CS,dc}^\sigma$ is the double-counting correction, which is needed to cancel the Coulomb interaction already included in the LSDA exchange-correlation potential. The form of the double-counting correction is not exactly known, and several approximations have been proposed and used in practice (see for example Ref.^{22,24,57,58}). We will return to this in Sec. II C after Eq. (22).

B. Dressed Green’s function and the local approximation

The interacting CS of Hamiltonian $\hat{H}^\sigma(\mathbf{k})_{CS,U}$ is described by the dressed Green’s function $\hat{G}_{CS}^\sigma(\mathbf{k}, \omega)$. This is defined via the Dyson equation

$$\bar{G}_{CS}^\sigma(\mathbf{k}, \omega) = [\bar{\mathcal{G}}_{CS}^\sigma(\mathbf{k}, \omega)^{-1} - \bar{\Sigma}_{CS}^\sigma(\mathbf{k}, \omega)]^{-1}, \quad (9)$$

where $\bar{\mathcal{G}}_{CS}^\sigma(\mathbf{k}, \omega)$ is the bare Green’s function of Eq. (4) and $\bar{\Sigma}_{CS}^\sigma(\mathbf{k}, \omega)$ is the retarded self-energy that needs to be calculated. We note that $\bar{\Sigma}_{CS}^\sigma(\mathbf{k}, \omega)$ is a $5N_{\text{TM}} \times 5N_{\text{TM}}$ frequency- and momentum-dependent matrix like the retarded CS Green’s function. To simplify the calculations, we here employ the DMFT approximation^{22,23}. We neglect off-diagonal matrix elements and the momentum-dependence, while we retain the frequency-dependence. This means that we set

$$\bar{\Sigma}_{CS}^\sigma(\mathbf{k}, \omega) \approx \text{diag}[\Sigma_{11}^\sigma(\omega), \dots, \Sigma_{i\lambda}^\sigma(\omega), \dots, \Sigma_{N_{\text{TM}}5}^\sigma(\omega)]. \quad (10)$$

The self-energy then needs to be evaluated via the self-consistent DMFT equations^{22,23}. Using as initial guess that $\bar{\Sigma}_{CS}^\sigma(\mathbf{k}, \omega) = 0$, we find that the DMFT equations converge in one iteration for the systems of interest here. Therefore, the local bare Green’s function

$$g_{i\lambda}^\sigma(\omega) = \frac{1}{N_{\mathbf{k}}} \sum_{\mathbf{k}} [\bar{\mathcal{G}}_{CS}^\sigma(\mathbf{k}, \omega)]_{i\lambda,i\lambda} \quad (11)$$

is employed to calculate the local self-energy $\Sigma_{i\lambda}^\sigma(\omega)$ (see next section); $N_{\mathbf{k}}$ is the number of \mathbf{k} -points. $\Sigma_{i\lambda}^\sigma(\omega)$ satisfies the Dyson equation

$$G_{i\lambda}^\sigma(\omega) = [g_{i\lambda}^\sigma(\omega)^{-1} - \Sigma_{i\lambda}^\sigma(\omega)]^{-1} \quad (12)$$

with

$$G_{i\lambda}^\sigma(\omega) \approx \frac{1}{N_{\mathbf{k}}} \sum_{\mathbf{k}} [\bar{\mathcal{G}}_{CS}^\sigma(\mathbf{k}, \omega)]_{i\lambda,i\lambda}. \quad (13)$$

After having solved the many-body problem for the CS, the self-energy can be expressed into SR basis as $\Sigma^\sigma(\mathbf{k}, \omega)$ by performing the inverse of the transformation

$$\Sigma^\sigma(\mathbf{k}, \omega) = W(\mathbf{k})^{-1\dagger} \begin{pmatrix} \bar{\Sigma}_{CS}^\sigma(\mathbf{k}, \omega) & 0 \\ 0 & 0 \end{pmatrix} W(\mathbf{k})^{-1}. \quad (14)$$

The SR dressed Green’s function is finally given by the equation

$$G^\sigma(\mathbf{k}, \omega) = [\mathcal{G}^\sigma(\mathbf{k}, \omega)^{-1} - \Sigma^\sigma(\mathbf{k}, \omega)]^{-1}. \quad (15)$$

and the density of states (DOS) at the energy E is defined as

$$\text{DOS}^\sigma(E) = -\frac{4\pi}{\hbar} \frac{1}{N_{\mathbf{k}}} \sum_{\mathbf{k}} \text{Im}[G^\sigma(\omega, \mathbf{k})], \quad (16)$$

where \hbar is the reduced Planck's constant. A systematic comparison of the DOS calculated by using DFT and our DMFT scheme will be presented in Sec. IV for Fe/W(110).

C. Self-energy in perturbation theory

We now describe in detail the method used to compute the self-energy $\Sigma_{i\lambda}^\sigma(\omega)$ in Eq. (12). In case of weakly or moderately correlated systems, such as the 3d ferromagnetic metals of interest here, the self-energy can be obtained using self-consistent perturbative approaches in terms of skeleton diagrams around the non-interacting solution. A popular scheme is the self-consistent fluctuating exchange approximation (FLEX)⁵⁹, which is conserving in the Baym-Kadanoff sense^{60–62}. The FLEX has been further combined with the T -matrix approximation, into the spin-polarized T -matrix fluctuating exchange approximation^{35–38}, the so-called SPT-FLEX impurity solver. The SPT-FLEX self-energy is described by the Hartree and Fock diagrams with the formal replacement of the bare interaction by the T -matrix^{63,64}, which obeys the Bethe-Salpeter-like integral equation. The SPT-FLEX is formulated on the imaginary (Matsubara) frequency axis and correlation functions are obtained indirectly via the numerical analytical continuation to the real frequency axis. Unfortunately, this often leads to numerical difficulties since the analytical continuation of discrete numerical data is not unambiguous and, in ad-

dition, it requires the treatment of the high-frequency “tails”⁶⁵. For this reason, we consider here a simpler second order perturbative treatment implemented to provide the self-energy directly on the real frequency axis, while retaining the multi-orbital nature of the many-body problem. The proposed approach represents a good compromise between the need for an accurate description of correlated effects and for a efficient and easy numerical evaluation of spectral properties.

The local retarded self-energy up to the second order in diagrammatic perturbation theory in U over the band width is written as

$$\Sigma_{i\lambda}^\sigma(\omega) \approx \Sigma_{i\lambda}^{\sigma(1)} + \Sigma_{i\lambda}^{\sigma(2)}(\omega). \quad (17)$$

The first-order contribution

$$\Sigma_{i\lambda}^{\sigma(1)} = \sum_{\lambda_1\sigma_1} U_{\lambda\lambda_1\lambda\lambda_1} n_{i\lambda_1}^{\sigma_1} - \sum_{\lambda_1} U_{\lambda\lambda_1\lambda_1\lambda} n_{i\lambda_1}^\sigma. \quad (18)$$

is the well-known Hartree-Fock approximation, where $n_{i\lambda}^\sigma = \int_{-\infty}^{\infty} d\omega f(\omega) \text{Im}g_{i\lambda}^\sigma(\omega)$ is the occupation of the orbital λ of spin σ at the atom i ; $f(\omega)$ is the Fermi function. $\Sigma_{i\lambda}^{\sigma(1)}$ is local in time, i.e. frequency independent. It therefore represents a one-electron potential producing only a shift of the non-interacting energy levels.

The derivation of the second order contributions is presented in the Appendix. It follows previous derivations seen in literature⁶⁶, and in particular Refs.^{45,46}. However, while those papers consider a single-orbital model⁴⁶ or an average interaction U (Ref.⁴⁵), we maintain a multi-orbital description including the complete four-index interaction. The resulting $\Sigma_{i\lambda}^{\sigma(2)}(\omega)$ is presented in Eqs. (A10) and (A10). It can be split into its real and imaginary part. The imaginary part is given by

$$\begin{aligned} \text{Im} \left[\Sigma_{i\lambda}^{\sigma(2)}(\omega) \right] &= -\pi \sum_{\lambda_1\lambda_2\lambda_3\sigma_1} U_{\lambda\lambda_1\lambda_2\lambda_3} U_{\lambda_3\lambda_2\lambda_1\lambda} \int_{-\infty}^{\infty} d\omega_1 \int_{-\infty}^{\infty} d\omega_2 D_{i\lambda_1}^{\sigma_1}(\omega_1) D_{i\lambda_2}^{\sigma}(\omega_2) D_{i\lambda_3}^{\sigma_1}(\omega_1 + \omega_2 - \omega) \times \\ &\quad \{f(\omega_1)f(\omega_2) + [1 - f(\omega_1) - f(\omega_2)] f(\omega_1 + \omega_2 - \omega)\} \\ &\quad + \pi \sum_{\lambda_1\lambda_2\lambda_3} U_{\lambda\lambda_1\lambda_2\lambda_3} U_{\lambda_2\lambda_3\lambda_1\lambda} \int_{-\infty}^{\infty} d\omega_1 \int_{-\infty}^{\infty} d\omega_2 D_{i\lambda_1}^{\sigma}(\omega_1 + \omega_2 - \omega) D_{i\lambda_2}^{\sigma}(\omega_2) D_{i\lambda_3}^{\sigma}(\omega_1) \times \\ &\quad \{f(\omega_2)f(\omega_1) + [1 - f(\omega_2) - f(\omega_1)] f(\omega_1 + \omega_2 - \omega)\}, \end{aligned} \quad (19)$$

where

$$D_{i\lambda}^\sigma(\omega) = -\frac{1}{\pi} \text{Im}[g_{i\lambda}^\sigma(\omega)] \quad (20)$$

is the spectral function of $g_{i\lambda}^\sigma(\omega)$. The real part is given by the Kramers-Kronig relations

$$\text{Re} \left[\Sigma_{i\lambda}^{\sigma(2)}(\omega) \right] = -\frac{1}{\pi} \int_{-\infty}^{\infty} d\omega' \frac{\text{Im} \left[\Sigma_{i\lambda}^{\sigma(2)}(\omega') \right]}{\omega - \omega'}. \quad (21)$$

Eqs. (19) and (21) are easily implemented thus allowing for the calculation of the second order self-energy contributions. The numerical integration over the frequencies ω_1 and ω_2 in Eq. (19) would potentially represent a computational bottleneck of the method if it was carried out using a too large number of discrete frequency points. However, in the case of ferromagnetic TMs, we find accurate results already for relatively coarse frequency grids

($d\omega \approx 10^{-3}$ eV/ \hbar) thus making the calculations computationally quite inexpensive.

D. Self-energy calculations combined with DFT

Having derived the self-energy, we now discuss how this is combined with DFT, how the first and second order contributions can be taken into account and how they are calculated in our implementation.

1. The reduction to LSDA+U

The first order term of Eq. (17) combined with DFT reduces to the LSDA+U approach. The double counting correction $H_{\text{CS},dc}^\sigma$ of Eq. (6) can be englobed into $\Sigma_{i\lambda}^{\sigma(1)}$ and can be approximated with one of the various forms proposed for LSDA+U⁶⁷. For example, using the so-called fully-localized limit⁶⁸ for $H_{\text{CS},dc}^\sigma$, leads to

$$\begin{aligned} \Sigma_{i\lambda,dc}^{\sigma(1)} &= \Sigma_{i\lambda}^{\sigma(1)} - H_{\text{CS},dc}^\sigma = \sum_{\lambda_1\sigma_1} U_{\lambda\lambda_1\lambda\lambda_1} n_{i\lambda_1}^{\sigma_1} \\ &\sum_{\lambda_1} U_{\lambda\lambda_1\lambda_1\lambda} - n_{i\lambda_1}^\sigma - \left[U \left(N_i - \frac{1}{2} \right) + J \sum_{\sigma} \left(N_i^\sigma - \frac{1}{2} \right) \right], \end{aligned} \quad (22)$$

where $N_i = \sum_{\sigma} N_i^\sigma = \sum_{\sigma\lambda} n_{i\lambda}^\sigma$ is the total occupation, and U and J are the average effective Coulomb and exchange interactions in Eqs. (7) and (8). $\Sigma_{i\lambda,dc}^{\sigma(1)}$ is exactly the Hubbard corrective potential of the LSDA+U Hamiltonian proposed by Lichtenstein *et al.* in Ref.¹⁶ [note that, differently from the original formulation, only diagonal elements of the density matrix $n_{i\lambda_1}^{\sigma_1}$ appear in Eq. (22) because we assumed $g_{i\lambda}^\sigma(\omega)$ in Eq. (11) to be diagonal in the orbital indices]. Based on these observations, we evaluate the first-order self-energy performing a standard LSDA+U calculation. Although, Eq. (22) is the most complete formulation of the LSDA+U Hubbard corrective potential with fully orbital-dependent electronic interactions, we used a simplified expression introduced by Dudarev *et al.*¹⁷

$$\Sigma_{i\lambda,dc}^{\sigma(1)} \approx V_{U,i\lambda}^\sigma = (U - J) \left(\frac{1}{2} - n_{i\lambda}^\sigma \right). \quad (23)$$

to reduce the complexity of the calculations. This simplified expression has been successfully applied in several studies and for most materials it yields similar results as the fully rotationally invariant formulation (see Ref.⁶⁷ and references therein for more details).

2. Σ_2 relative to HF: the LSDA+ Σ_2

The fact that the Hartree-Fock self-energy is static leaves us the freedom to chose how to practically perform the perturbative calculations up to second order.

Namely, starting from the non-interacting Green's function $g_{i\lambda}^\sigma(\omega)$ of Eq. (11) we can calculate the total self-energy corrections up to second order, i.e. including the static $\Sigma_{i\lambda}^{\sigma(1)}$ and the dynamic $\Sigma_{i\lambda}^{\sigma(2)}(\omega)$ contributions. Alternatively, we can "immerse" the static contribution, approximated as in Eq. (23), into the non-interacting local Green's functions. This means that $g_{i\lambda}^\sigma(\omega)$ is replaced by the LSDA+U Green's function

$$g_{\text{LSDA+U},i\lambda}^\sigma(\omega) = [g_{i\lambda}^\sigma(\omega)^{-1} - V_{U,i\lambda}^\sigma]^{-1}. \quad (24)$$

The Dyson Eq. (12) retains its structure with the total self-energy $\Sigma_{i\lambda}^\sigma(\omega)$ substituted by the correlation self-energy $\Sigma_{C,i\lambda}^\sigma(\omega) = \Sigma_{i\lambda}^\sigma(\omega) - V_{U,i\lambda}^\sigma$, where $\Sigma_{C,i\lambda}^\sigma(\omega)$ is evaluated using the LSDA+U Green's functions $g_{\text{LSDA+U},i\lambda}^\sigma(\omega)$.

Following these considerations, our calculations are practically carried out by first performing fully charge self-consistent LSDA+U calculations to obtain the Green's functions $g_{\text{LSDA+U},i\lambda}^\sigma(\omega)$, which already contains the Hartree-Fock part. Subsequently these are used to compute the second order self-energy corrections only, i.e. just the dynamic $\Sigma_{i\lambda}^{\sigma(2)}(\omega)$ contributions. We refer to this method as LSDA+ Σ_2 . We note that, LSDA+ Σ_2 can in principle, be extended in a fully charge self-consistent way which requires updating the occupation matrix. This may be investigated in future studies.

III. COMPUTATIONAL DETAILS

We treat core electrons with norm-conserving Troullier-Martin pseudopotentials. The valence states are expanded through a numerical atomic orbital basis set including multiple- ζ and polarized functions⁵¹. The electronic temperature is set to 300 K. The real space mesh is set by an equivalent energy cutoff of 300 Ry. We use 15×15 \mathbf{k} -point mesh to compute the self-consistent charge density with LSDA(+U). This charge density is then used as input in a non-self-consistent calculation to obtain the density of states employing 61×61 \mathbf{k} -points. We shift all energies in such a way to set the Fermi level at 0 eV. To calculate the second-order self-energy, we use a frequency grid comprising 4400 points and extending from -16 to 6 eV/ \hbar . The imaginary part η in Eq. (1) is 0.01 eV/ \hbar and 0.005 eV/ \hbar in LSDA(+U) and in LSDA+ Σ_2 calculations, respectively. This leads to an additional broadening of the DOS for a better display in Figs. 2 and 3.

We express the Coulomb parameters $U_{\lambda_1,\lambda_2,\lambda_3,\lambda_4}$ in terms of Slater integrals F^0 , F^2 and F^4 (Ref. 14). These are connected to the average effective Coulomb and exchange interactions of Eqs. (7) and (8) through the relations $U = F^0$ and $J = (F^2 + F^4)/14$. The ratio F^4/F^2 is assumed to correspond to the atomic value ≈ 0.625 ⁶⁹.

IV. RESULTS

To describe the performances of our method we consider a monolayer of Fe on a W(110) substrate, a systems quite investigated in nanoscale magnetism and often used in spin-polarized scanning tunneling experiments^{47,48}. We neglect the spin-orbit coupling, which leads to strong magnetocrystalline anisotropy⁷⁰ and, according to recent studies, is responsible for the Dzyaloshinskii-Moriya interaction and eventually exotic magnetic orders⁷¹. We focus instead on electron correlation spectral features modeled by DFT+ Σ_2 . To our knowledge there are no high quality photoemission spectroscopy data allowing a direct comparison between theory and experiments. We therefore discuss general trends in the results obtained with our method.

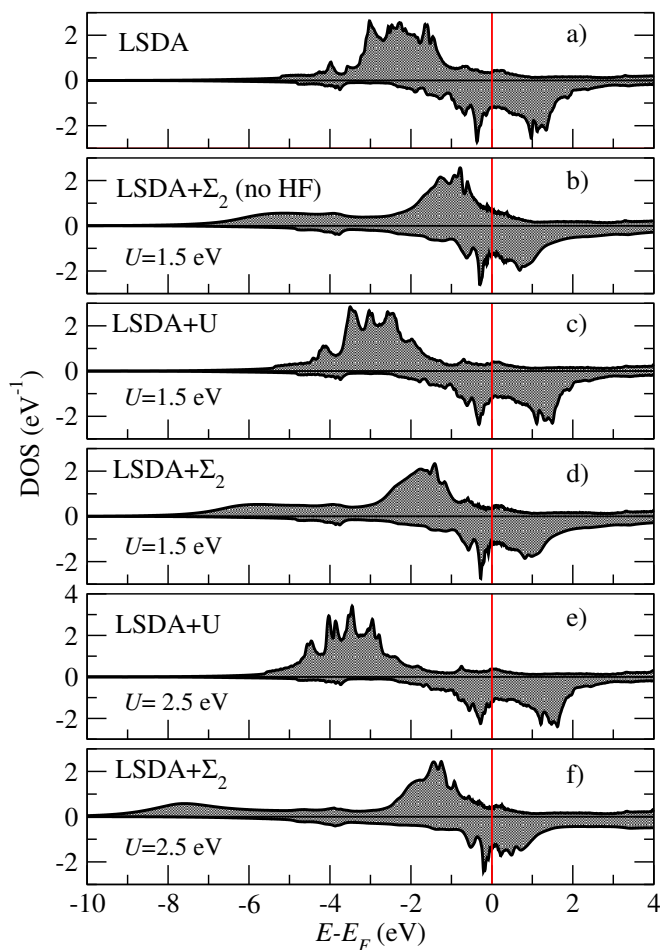


FIG. 2: DOS of one of the Fe atoms calculated by means of LSDA, LSDA+U and LSDA+ Σ_2 . The Fermi level is at 0 eV. The value of U used in LSDA+U is indicated. $J = 0.5$ eV in all calculations. LSDA+ Σ_2 (no HF) indicates calculations where the approximate HF potential of Eq. 23 is neglected.

We model the Fe/W(110) surface as shown in Fig. 1. Its rectangular unit cell contains two symmetrically equivalent Fe atoms, whose $3d$ orbitals form the corre-

lated subspace of total dimension of 20. The Fe DOS calculated by means of LSDA, LSDA+U and LSDA+ Σ_2 is presented in Fig. 2. A careful inspection allows us to understand the effect of the dynamical self-energy compared to different mean-field static approximations. LSDA produces a splitting between the spin up (majority) and spin down (minority) bands of about 2 eV (Fig. 2-a). Comparing with the orbital resolved DOS in Fig. 3, we find that the prominent peaks for both spin channels have mostly d character. The total DOS for the spin up channel is centered at $E - E_F \approx -2.2$ eV and is almost completely filled. The total occupation of the majority d orbitals is 4.68 electrons. In contrast, the spin down DOS presents two main peaks at the opposite sides of the Fermi level and separated by a pseudo-gap. As seen in the orbital-resolved DOS in Fig. 3, the two-peak structure reflects the separation of the Fe d_{xy} and d_{yz} orbitals from the d_{xz} , d_{z^2} and $d_{x^2-y^2}$ due to the (110) surface symmetry. The d_{xy} orbitals are oriented along the crystal direction connecting the surface Fe atoms and thus merge into σ bonding and anti-bonding bands. The Fe d_{yz} orbitals overlap with the $5d_{yz}$ orbitals of the W atoms underneath the surface forming a second set of σ bonding and anti-bonding bands. All bonding states are centered at about $E - E_F \approx -0.7$ eV giving the first sharp peak in the spin down DOS, while the antibonding states are unoccupied and emerge as very broad features extending up to 2 eV. The d_{xz} , d_{z^2} and $d_{x^2-y^2}$ orbitals mostly overlap with s orbitals forming broad states centered around $E - E_F \approx 1.15$ eV. They contribute to the second unoccupied peak in the spin down DOS. The occupation of the Fe d_{xy} and d_{yz} orbitals is about 0.46, whereas that of the d_{xz} , d_{z^2} and $d_{x^2-y^2}$ orbitals is 0.31, contributing to the total occupation of the minority d states equal to 1.86 electrons. The spin magnetic moment is $2.84 \mu_B$, considerably enhanced with respect to that in bulk Fe, $2.2 \mu_B$.

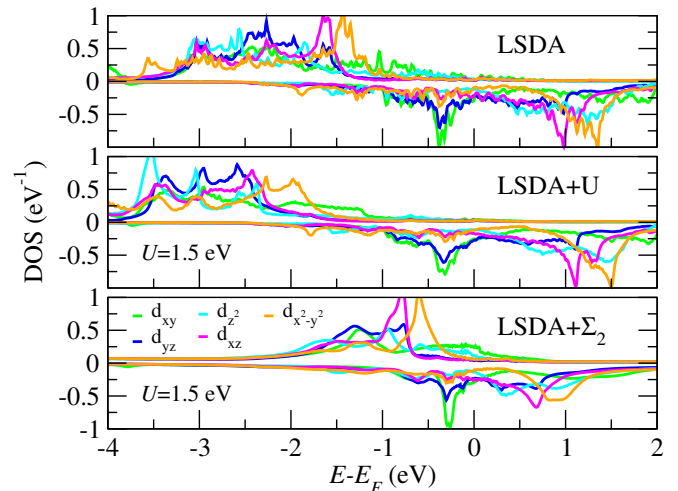


FIG. 3: Orbital resolved DOS of Fe atom obtained via LSDA and LSDA+ Σ_2 calculations. The Fermi level is at 0 eV.

The DOS calculated by means of LSDA+U is shown in Fig. 2-c and -e for $U = 1.5$ eV and $U = 2.5$ eV, respectively, and $J = 0.5$ eV. In such a mean-field like approach the $V_{U,i\lambda}^\sigma$ potential shifts the spin up LSDA DOS towards lower energies by about $-0.5(U - J)$ [see Eq. (23)]. The occupation of the spin up states therefore increases as a function of U . In contrast, the $V_{U,i\lambda}^\sigma$ potential barely affects the spin down d_{xy} and d_{yz} orbitals and moves the d_{xz} , d_{z^2} and $d_{x^2-y^2}$ orbitals towards higher energies by about $0.2(U - J)$. The pseudo-gap in the spin down DOS across the Fermi level widens, while the d_{xz} , d_{z^2} and $d_{x^2-y^2}$ orbitals are slightly emptied. Overall, the splitting between the spin up and down DOS becomes larger and, as a result, the total Fe magnetic moment systematically increases as a function of $U - J$. This is a general outcome of DFT+U calculations found for all ferromagnetic materials¹⁸. It is a consequence of the fact that the $V_{U,i\lambda}^\sigma$ potential of Eqs. (22) and (23) represents the Hartree-Fock approximation to the Hubbard interaction.

Next, we discuss the results obtained including second order self-energy contributions. These are shown in Fig. 2-b, -d and -f. We use $U = 1.5$ eV and $U = 2.5$ eV and $J = 0.5$ eV like in the LSDA+U calculations. Since the LSDA d bandwidth is about 4 eV, the perturbation expansion is valid. The calculations in Fig. 2-d and -f are performed as explained at the end of Sec. IID 2. The calculations in Fig. 2-b, which are indicated as “LSDA+ Σ_2 (no HF)”, are carried out neglecting the approximate Hartree-Fock potential of Eq. (23) and using the LSDA Green’s function to evaluate second order self-energy contributions. The main features due to the second order self-energy are similar across Fig. 2-b, -d and -f. Some redistribution of the spectral weight occurs resulting in a considerable spectral narrowing. The orbital ordering (orbitals’ position in energy) and the character of the main peaks recognizable in Fig. 3 is preserved as it is dictated by the surface symmetry and the crystal field. The changes in the DOS are more pronounced for spin up than for spin down. The top of the occupied d DOS in the spin up channel is shifted towards the Fermi level, while the down DOS is barely affected. This leads to a lowering of the Fe magnetic moment μ reported in Tab. I. For $U = 2.5$ eV, we observe a reduction in excess of $0.3\mu_B$ compared to LSDA+U thus demonstrating that correlation effects play a crucial role in counterbalancing the exchange interaction. This can be easily understood by inspecting the mathematical form of the second order self-energy of Eq. (19) or the corresponding Feynman diagrams in the appendix. Electronic correlations are build-up by the scattering processes between electrons and electron-hole pairs. Since the spin up channel is essentially full, electron-hole pairs are mostly created in the spin down channel. Therefore a spin up electron will more likely scatter with an opposite-spin pair costing an effective interaction U . In contrast, a spin down electron will scatter with same-spin pairs with effective interaction $U - J < U$. Therefore, correlation effects are stronger for spin up than for spin down electrons.

Method	n_\uparrow	n_\downarrow	μ
LSDA	4.68	1.85	2.84
LSDA+ Σ_2 (no HF)	4.52	1.91	2.6
LSDA+U ($U = 1.5$)	4.75	1.75	3.0
LSDA+ Σ_2 ($U = 1.5$)	4.69	1.81	2.88
LSDA+U ($U = 2.5$)	4.79	1.69	3.1
LSDA+ Σ_2 ($U = 1.5$)	4.65	1.88	2.76

TABLE I: Total d orbitals occupation and magnetic moment $\mu = n_\uparrow - n_\downarrow$ (in Bohr magneton μ_B .)

Analyzing in more details the results, we see that, for $U = 1.5$ eV, the spin up d DOS center is at $E - E_F \approx 1.5$ eV and at ≈ 2.0 eV in Fig. 2-b and 2-d, respectively. Clearly the differences in the two cases can be interpreted as due to the initial state dependence of perturbation theory and they reflect the differences between the LSDA and LSDA+U DOS. In spite of that, the two results are overall quite similar. The interaction strength $U = 1.5$ eV is comparable to the spin-splitting of the LSDA d bands, or, in other words, to the Stoner parameter evaluated from the LSDA band structure^{72,73}. In general, we find that whenever U is comparable to the LSDA Stoner parameter, neglecting the HF potential and using the LSDA Green’s function to compute $\Sigma_{i\lambda}^{\sigma(2)}(\omega)$ is a practically reliable simplification.

We now compare the LSDA+ Σ_2 results for $U = 1.5$ eV and for $U = 2.5$ eV (Fig. 2-d and -f). We see that a larger U does not significantly change the position of the d states, but it induces a narrowing of both the spin up and the spin down DOS features. According to this finding, an increase in the local Coulomb parameter U including dynamic self-energy effects leads to a re-shaping of the spectrum rather than in a modification of their spin-splitting as one would expect based on a static mean-field picture.

Far from the Fermi level, we distinguish a satellite appearing in the spin-up channel below -4 eV. A similar feature has been unequivocally observed in photoemission measurements for Ni¹³ and it has been predicted for bulk Fe as well²⁵. Here we show that it is present even in a Fe monolayer. This a solid prediction of an intrinsic many-body spectroscopic feature that, we hope, will be identified in experiments. As already noted in Ref.²⁵ for bulk calculations, the center of the satellite systematically shifts towards lower energies when increasing U .

Since the crystal-field splitting is rather small, the self-energy is very similar for all orbitals. Thus, we present in Fig. 4 the self-energy averaged over the orbital indexes. The overall shape of the real and imaginary parts is typical of ferromagnetic transition metals²⁵. For example, in Fig. 4-a we note that, in the spin up channel, the real part of the self-energy is positive in the energy range between -4.3 eV and the Fermi level, and it shows a maximum at about $E - E_F \approx -2.7$ eV. This causes the shift of occupied d states towards to the Fermi level as observed in Fig. 2. In contrast, for energies below -4.3 eV, the negative real part of the self-energy draws the spectral

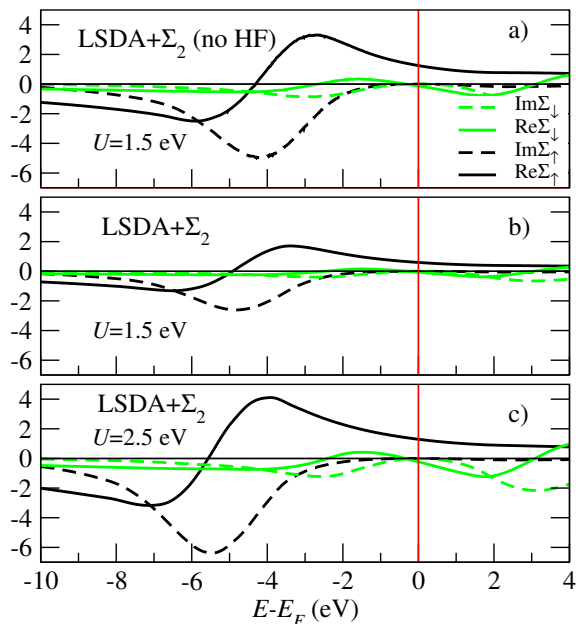


FIG. 4: Real and imaginary part of the self-energy (in eV) averaged over the orbital index.

weight towards lower energies leading to the formation of the satellite in the DOS. The imaginary part has an extended negative peak centered at $E - E_F \approx -5$ eV resulting in the large broadening of the satellite. In the spin down channel, correlation effects are much less pronounced and both the real and imaginary part of the self-energy are quite small. Similar results are found in Fig. 4-a, -b and -c. However, we observe that both the real and imaginary part of the self-energy are smaller in Fig. 4-b and -c. This is consistent with the previous observation that the DOS in Fig. 2-d appears less shifted and less narrow than in Fig. 2-b. For larger U values, such as 2.5 eV (Fig. 4-c), the peak in the real part of the self-energy for spin up is enhanced to compensate the large U potential, which brings the spin up d states towards too low energies.

The self-energy near the Fermi level has Fermi-liquid character: for the imaginary part, we have $-\text{Im}\Sigma_\sigma(E) \propto (E - E_F)^2$, whereas the real part has negative slope, $\partial/\partial E(\text{Re}\Sigma_\sigma(E)) < 0$. We then evaluate the mass enhancement, which amounts to

$$\left(\frac{m^*}{m}\right)_{\lambda,\sigma} = 1 - \frac{\partial}{\partial E}(\text{Re}\Sigma_{\lambda,\sigma}(E)) \quad (25)$$

where m represents the band-mass obtained within the LSDA(+U) calculations. The enhancement factors with respect to LSDA are very similar for all d orbitals and spin channels. They are on average about 1.2, which indicates that the system is medium-correlated. The mass enhancement increases as a function of U . Interestingly, in case of $U = 2.5$ eV, m^*/m becomes larger for spin down (1.3) than spin up orbitals (1.8). Although the position of the spin down d orbitals is less affected by the

self-energy than that of spin up orbitals, the spin down DOS is considerably narrowed at the Fermi energy as already observed in Fig. 2-f.

Summarizing, our results demonstrate that the second order self-energy added to DFT captures the general correlation effects expected in TMs and improves the description of quasi-particle excitations. In particular it corrects the well-known problem that LSDA(+U) overestimates the spin-splitting of the $3d$ states. Unfortunately, no spectroscopic results are available and our assessment is limited to qualitative considerations. We note that the DOS spin-polarization of Fe/W(110) can be directly probed in spin-polarized STM experiments⁷⁴. Comparing the results of DFT+ Σ_2 calculations to such experiments may represent an interesting outlook for future studies.

V. CONCLUSIONS

DFT+ Σ_2 combines DFT to a multi-orbital solver for the Hubbard model, where the Coulomb interaction parameter U is treated in perturbation theory up to second order. The method provides a realistic description of moderately correlated materials, and our implementation is particularly suited to investigate TM surfaces and interfaces. As an example of application, we considered a Fe monolayer on a W(110) substrate. We discussed in detail the correlated DOS comparing the results with those of LSDA and LSDA+U calculations. We found that second order self-energy contributions led to a shift of the majority-spin DOS towards the Fermi level and therefore to a reduction of the d states spin splitting compared to LSDA calculations. Furthermore, we predicted a satellite appearing in an energy range between 5 and 8 eV below the Fermi level. This is a notable spectroscopic feature that may be identified by photoemission experiments. The use of different unperturbed states and the inclusion of the first-order contribution in DFT+ Σ_2 gave differences in the DOS spin splitting and spectral width. These differences were nonetheless rather minor in cases, where U was comparable to the Stoner interaction parameter evaluated from the LSDA band structures.

In our calculations we employed the local approximation thus we neglected spatially non-local correlation effects. However, the method can in principle be extended to allow for momentum and frequency dependent self-energies, although this would increase significantly the complexity of the numerical implementation and the computational overhead.

Overall, our implementation of DFT+ Σ_2 can be readily used to simulate, at a relatively low computational cost, correlation effects in the electronic structure of heterostructures comprising TMs. The calculation of the self-energy on the real frequency axis is particularly convenient if one is interested to treat charge and spin transport properties using generalized Landauer methods^{42,43}, which require the evaluation of the frequency depen-

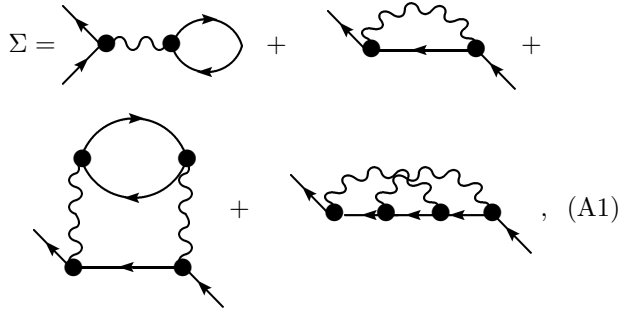
dent transmission function^{33,44}. As such, we believe that DFT+ Σ_2 will provide important theoretical inputs for the design of materials and devices for electronics and spintronics.

VI. ACKNOWLEDGEMENTS

AD and AH acknowledge funding by the Science Foundation Ireland (SFI) and the Royal Society through the University Research Fellowship URF-R1-191769. MMR acknowledges funding provided by the Institute of Physics Belgrade, through the grant by the Ministry of Education, Science, and Technological Development of the Republic of Serbia. IR acknowledges the support of the UK government department for Business, Energy and Industrial Strategy through the UK national quantum technologies programme. LC acknowledges the financial support by the Deutsche Forschungsgemeinschaft through TRR80 (project F6) Project number 107745057. Computational resources were provided by Trinity College Dublin Research IT.

Appendix A: Second order self-energy

We provide here details about the perturbative treatment of the multi-orbital electronic system. We use the Keldysh Green's functions formalism⁶². The self-energy, up to second order can be schematically expressed with the Feynman diagrams



where the dots represents space-(contour time) coordinates, the straight line represents the Green's function and the wiggly lines represents the interaction. Converted into equations these diagrams give four contribu-

tions to the self-energy

$$\begin{aligned} \Sigma_{\lambda\sigma}^{(1,1)}(\mathbf{k}; t, t') = & \\ -i\delta_C(t, t') \sum_{\lambda_f, \sigma_f} \tilde{U}_{\lambda\lambda_f\lambda\lambda_f}^{\sigma\sigma_f\sigma\sigma_f}(0; t) \sum_{\mathbf{p}} g_{\lambda_f\sigma_f}(\mathbf{p}; t, t), \end{aligned} \quad (\text{A2})$$

$$\begin{aligned} \Sigma_{\lambda\sigma}^{(1,2)}(\mathbf{k}; t, t') = & \\ i\delta_C(t, t') \sum_{\lambda_f} \tilde{U}_{\lambda\lambda_f\lambda_f\lambda}^{\sigma\sigma\sigma\sigma}(\mathbf{k} - \mathbf{p}; t) \sum_{\mathbf{p}} g_{\lambda_f\sigma}(\mathbf{p}; t, t'), \end{aligned} \quad (\text{A3})$$

$$\begin{aligned} \Sigma_{\lambda_a\lambda_d\sigma_a\sigma_d}^{(2,1)}(\mathbf{k}; t, t') = & \\ \sum_{\lambda_b, \lambda_e, \lambda_f, \sigma_f} \tilde{U}_{\lambda_a\lambda_e\lambda_b\lambda_f}^{\sigma_a\sigma_f\sigma_a\sigma_f}(\mathbf{q}; t) \tilde{U}_{\lambda_f\lambda_b\lambda_e\lambda_d}^{\sigma_f\sigma_a\sigma_f\sigma_a}(\mathbf{q}; t') \delta_{\sigma_a\sigma_d} & \\ \sum_{\mathbf{p}, \mathbf{q}} g_{\lambda_b\sigma_a}(\mathbf{k} + \mathbf{q}; t, t') g_{\lambda_f\sigma_f}(\mathbf{p}; t', t) g_{\lambda_e\sigma_f}(\mathbf{p} - \mathbf{q}; t, t'), \end{aligned} \quad (\text{A4})$$

$$\begin{aligned} \Sigma_{\lambda_a\lambda_d\sigma_a\sigma_d}^{(2,2)}(\mathbf{k}; t, t') = & \\ - \sum_{\lambda_b, \lambda_c, \lambda_e} \tilde{U}_{\lambda_a\lambda_e\lambda_c\lambda_b}^{\sigma_a\sigma_a\sigma_a\sigma_a}(\mathbf{p}; t) \tilde{U}_{\lambda_c\lambda_b\lambda_e\lambda_d}^{\sigma_a\sigma_a\sigma_a\sigma_a}(\mathbf{q}; t') \delta_{\sigma_a\sigma_d} & \\ \sum_{\mathbf{p}, \mathbf{q}} g_{\lambda_b\sigma_a}(\mathbf{k} - \mathbf{q}; t, t') g_{\lambda_c\sigma_a}(\mathbf{k} - \mathbf{p} - \mathbf{q}; t', t) g_{\lambda_e\sigma_a}(\mathbf{k} - \mathbf{p}; t, t'). \end{aligned} \quad (\text{A5})$$

In the specific case of the Hubbard model, the interaction matrix \tilde{U} is time and momentum independent and we refer to it as U in the main text. Additionally, the Hubbard U matrix is also spin independent, but, in this appendix, we keep the spin indices in accordance with the most general notation.

After applying the Langreth rules⁶² and performing the Fourier transform we obtain the first order terms

$$\Sigma_{\lambda\sigma}^{(1,1)r}(\mathbf{k}; \omega) = -i \sum_{\lambda_f, \sigma_f} U_{\lambda\lambda_f\lambda\lambda_f}^{\sigma\sigma_f\sigma\sigma_f} \sum_{\mathbf{p}} \int \frac{d\omega_1}{2\pi} g_{\lambda_f\sigma_f}^<(\mathbf{p}; \omega_1), \quad (\text{A6})$$

$$\Sigma_{\lambda\sigma}^{(1,2)r}(\mathbf{k}; \omega) = i \sum_{\lambda_f} U_{\lambda\lambda_f\lambda_f\lambda}^{\sigma\sigma\sigma\sigma} \sum_{\mathbf{p}} \int \frac{d\omega_1}{2\pi} g_{\lambda_f\sigma_f}^<(\mathbf{p}; \omega_1), \quad (\text{A7})$$

where the lesser Green's function in equilibrium assumes the following form

$$g_{\lambda\sigma}^<(\omega) = -2if(\omega) \text{Im} g_{\lambda\sigma}^r(\omega), \quad (\text{A8})$$

with $g_{\lambda\sigma}^r(\omega)$ the retarded Green's function and $f(\omega)$ the Fermi function. The first order terms can then be written in well known Hartree-Fock expression of Eq. (18).

The two second order terms giving reads

$$\begin{aligned} \Sigma_{\lambda_a \lambda_d \sigma \sigma}^{(2,1)r}(\mathbf{k}; \omega) = & \sum_{\lambda_b, \lambda_e, \lambda_f, \sigma_f} U_{\lambda_a \lambda_e \lambda_b \lambda_f}^{\sigma \sigma_f \sigma \sigma_f} U_{\lambda_f \lambda_b \lambda_e \lambda_d}^{\sigma \sigma_f \sigma \sigma_f} \sum_{\mathbf{p}, \mathbf{q}} \int_{-\infty}^{\infty} \frac{d\omega_1}{2\pi} \int_{-\infty}^{\infty} \frac{d\omega_2}{2\pi} [\\ & g_{\lambda_b \sigma}^{\leftarrow}(\mathbf{k} + \mathbf{q}; \omega + \omega_1) g_{\lambda_f \sigma_f}^{\leftarrow}(\mathbf{p}; \omega_2) g_{\lambda_e \sigma_f}^r(\mathbf{p} - \mathbf{q}; \omega_2 - \omega_1) \\ & + g_{\lambda_b \sigma}^r(\mathbf{k} + \mathbf{q}; \omega + \omega_1) g_{\lambda_f \sigma_f}^{\leftarrow}(\mathbf{p}; \omega_2) g_{\lambda_e \sigma_f}^{\leftarrow}(\mathbf{p} - \mathbf{q}; \omega_2 - \omega_1) \\ & + g_{\lambda_b \sigma}^r(\mathbf{k} + \mathbf{q}; \omega + \omega_1) g_{\lambda_f \sigma_f}^{\leftarrow}(\mathbf{p}; \omega_2) g_{\lambda_e \sigma_f}^r(\mathbf{p} - \mathbf{q}; \omega_2 - \omega_1) \\ & + g_{\lambda_b \sigma}^{\leftarrow}(\mathbf{k} + \mathbf{q}; \omega + \omega_1) g_{\lambda_f \sigma_f}^A(\mathbf{p}; \omega_2) g_{\lambda_e \sigma_f}^{\leftarrow}(\mathbf{p} - \mathbf{q}; \omega_2 - \omega_1)] \end{aligned} \quad (\text{A9})$$

$$\begin{aligned} \Sigma_{\lambda_a \lambda_d \sigma \sigma}^{(2,2)r}(\mathbf{k}; \omega) = & - \sum_{\lambda_b, \lambda_c, \lambda_e} U_{\lambda_a \lambda_e \lambda_c \lambda_b}^{\sigma \sigma \sigma \sigma} U_{\lambda_c \lambda_b \lambda_e \lambda_d}^{\sigma \sigma \sigma \sigma} \sum_{\mathbf{p}, \mathbf{q}} \int_{-\infty}^{\infty} \frac{d\omega_1}{2\pi} \int_{-\infty}^{\infty} \frac{d\omega_2}{2\pi} [\\ & g_{\lambda_b \sigma}^{\leftarrow}(\mathbf{k} + \mathbf{q}; \omega - \omega_2) g_{\lambda_e \sigma}^{\leftarrow}(\mathbf{p}; \omega_2) g_{\lambda_c \sigma}^r(\mathbf{p} - \mathbf{q}; \omega_2 - \omega_1) \\ & + g_{\lambda_b \sigma}^r(\mathbf{k} + \mathbf{q}; \omega - \omega_2) g_{\lambda_e \sigma}^{\leftarrow}(\mathbf{p}; \omega_2) g_{\lambda_c \sigma}^{\leftarrow}(\mathbf{p} - \mathbf{q}; \omega_2 - \omega_1) \\ & + g_{\lambda_b \sigma}^r(\mathbf{k} + \mathbf{q}; \omega - \omega_2) g_{\lambda_e \sigma}^{\leftarrow}(\mathbf{p}; \omega_2) g_{\lambda_c \sigma}^r(\mathbf{p} - \mathbf{q}; \omega_2 - \omega_1) \\ & + g_{\lambda_b \sigma}^{\leftarrow}(\mathbf{k} + \mathbf{q}; \omega - \omega_2) g_{\lambda_e \sigma}^A(\mathbf{p}; \omega_2) g_{\lambda_c \sigma}^{\leftarrow}(\mathbf{p} - \mathbf{q}; \omega_2 - \omega_1)]. \end{aligned} \quad (\text{A10})$$

After a few steps of algebra and neglecting the momentum dependence, we easily obtain Eq. (19). We note that we drop the superscript “r” for “retarded” in the main text to keep the notation lighter.

* andrea.droghetti@tcd.ie

- ¹ C. Tusche, M. Ellguth, V. Feyer, A. Krasyuk, C. Wiemann, J. Henk, C. M. Schneider, and J. Kirschner, *Nat. Commun.* **9**, 3727 (2018), URL <https://doi.org/10.1038/s41467-018-05960-5>.
- ² R. Wiesendanger, *Rev. Mod. Phys.* **81**, 1495 (2009), URL <https://link.aps.org/doi/10.1103/RevModPhys.81.1495>.
- ³ R. O. Jones and O. Gunnarsson, *Rev. Mod. Phys.* **61**, 689 (1989), URL <http://link.aps.org/doi/10.1103/RevModPhys.61.689>.
- ⁴ W. Kohn, *Rev. Mod. Phys.* **71**, 1253 (1999).
- ⁵ R. O. Jones, *Rev. Mod. Phys.* **87**, 897 (2015), URL <http://link.aps.org/doi/10.1103/RevModPhys.87.897>.
- ⁶ U. von Barth and L. Hedin, *J. Phys. C* **5**, 1629 (1972).
- ⁷ S. H. Vosko, L. Wilk, and M. Nusair, *Can. J. Phys.* **58**, 1200 (1980).
- ⁸ J. P. Perdew, J. A. Chevary, S. H. Vosko, K. A. Jackson, M. R. Pederson, D. J. Singh, and C. Fiolhais, *Phys. Rev. B* **46**, 6671 (1992), URL <https://link.aps.org/doi/10.1103/PhysRevB.46.6671>.
- ⁹ J. P. Perdew, J. A. Chevary, S. H. Vosko, K. A. Jackson, M. R. Pederson, D. J. Singh, and C. Fiolhais, *Phys. Rev. B* **48**, 4978 (1993), URL <https://link.aps.org/doi/10.1103/PhysRevB.48.4978.2>.
- ¹⁰ J. P. Perdew, K. Burke, and M. Ernzerhof, *Phys. Rev. Lett.* **77**, 3865 (1996), URL <https://link.aps.org/doi/10.1103/PhysRevLett.77.3865>.
- ¹¹ S. Monastra, F. Manghi, C. A. Rozzi, C. Arcangeli, E. Wetli, H.-J. Neff, T. Greber, and J. Osterwalder, *Phys. Rev. Lett.* **88**, 236402 (2002), URL <https://link.aps.org/doi/10.1103/PhysRevLett.88.236402>.
- ¹² J. Braun, J. Minár, H. Ebert, M. I. Katsnelson, and A. I. Lichtenstein, *Phys. Rev. Lett.* **97**, 227601 (2006), URL <https://link.aps.org/doi/10.1103/PhysRevLett.97.227601>.
- ¹³ C. Guillot, Y. Ballu, J. Paigné, J. Lecante, K. P. Jain, P. Thiry, R. Pinchaux, Y. Pétrouff, and L. M. Falicov, *Phys. Rev. Lett.* **39**, 1632 (1977), URL <https://link.aps.org/doi/10.1103/PhysRevLett.39.1632>.
- ¹⁴ M. Imada, A. Fujimori, and Y. Tokura, *Rev. Mod. Phys.* **70**, 1039 (1998).
- ¹⁵ V. I. Anisimov, J. Zaanen, and O. K. Andersen, *Phys. Rev. B* **44**, 943 (1991), URL <https://link.aps.org/doi/10.1103/PhysRevB.44.943>.
- ¹⁶ A. I. Lichtenstein, V. I. Anisimov, and J. Zaanen, *Phys. Rev. B* **52**, R5467 (1995), URL <https://link.aps.org/doi/10.1103/PhysRevB.52.R5467>.
- ¹⁷ S. L. Dudarev, G. A. Botton, S. Y. Savrasov, C. J. Humphreys, and A. P. Sutton, *Phys. Rev. B* **57**, 1505 (1998), URL <https://link.aps.org/doi/10.1103/PhysRevB.57.1505>.
- ¹⁸ M. Cococcioni and S. de Gironcoli, *Phys. Rev. B* **71**, 035105 (2005), URL <https://link.aps.org/doi/10.1103/PhysRevB.71.035105>.
- ¹⁹ W. Metzner and D. Vollhardt, *Phys. Rev. Lett.* **62**, 324 (1989).
- ²⁰ A. Georges, G. Kotliar, W. Krauth, and M. J. Rozenberg, *Rev. Mod. Phys.* **68**, 13 (1996).
- ²¹ G. Kotliar and D. Vollhardt, *Phys. Today* **57**, 53 (2004).
- ²² G. Kotliar, S. Y. Savrasov, K. Haule, V. S. Oudovenko, O. Parcollet, and C. A. Marianetti, *Rev. Mod. Phys.* **78**, 865 (2006).
- ²³ K. Held, *Adv. Phys.* **56**, 829 (2007).
- ²⁴ A. I. Lichtenstein, M. I. Katsnelson, and G. Kotliar, *Phys. Rev. Lett.* **87**, 067205 (2001).
- ²⁵ A. Grechnev, I. Di Marco, M. I. Katsnelson, A. I. Lichtenstein, J. M. Wills, and O. Eriksson, *Phys. Rev. B*

- 76, 035107 (2007), URL <https://link.aps.org/doi/10.1103/PhysRevB.76.035107>.
- ²⁶ A. Östlin, L. Vitos, and L. Chioncel, Phys. Rev. B **98**, 235135 (2018), URL <https://link.aps.org/doi/10.1103/PhysRevB.98.235135>.
- ²⁷ M. I. Katsnelson, V. Y. Irkhin, L. Chioncel, A. I. Lichtenstein, and R. A. de Groot, Rev. Mod. Phys. **80**, 315 (2008), URL <https://link.aps.org/doi/10.1103/RevModPhys.80.315>.
- ²⁸ F. Beiușeanu, C. Horea, E.-V. Macocian, T. Jurcuț, L. Vitos, and L. Chioncel, Phys. Rev. B **83**, 125107 (2011), URL <https://link.aps.org/doi/10.1103/PhysRevB.83.125107>.
- ²⁹ L. Chioncel, I. Leonov, H. Allmaier, F. Beiușeanu, E. Arrigoni, T. Jurcuț, and W. Pötz, Phys. Rev. B **83**, 035307 (2011), URL <https://link.aps.org/doi/10.1103/PhysRevB.83.035307>.
- ³⁰ I. Di Marco, A. Held, S. Keshavarz, Y. O. Kvashnin, and L. Chioncel, Phys. Rev. B **97**, 035105 (2018), URL <https://link.aps.org/doi/10.1103/PhysRevB.97.035105>.
- ³¹ S. Keshavarz, I. Di Marco, D. Thonig, L. Chioncel, O. Eriksson, and Y. O. Kvashnin, Phys. Rev. Materials **4**, 021401 (2020), URL <https://link.aps.org/doi/10.1103/PhysRevMaterials.4.021401>.
- ³² L. Chioncel, M. I. Katsnelson, G. A. de Wijs, R. A. de Groot, and A. I. Lichtenstein, Phys. Rev. B **71**, 085111 (2005), URL <https://link.aps.org/doi/10.1103/PhysRevB.71.085111>.
- ³³ L. Chioncel, C. Morari, A. Östlin, W. H. Appelt, A. Droghetti, M. M. Radonjić, I. Rungger, L. Vitos, U. Eckern, and A. V. Postnikov, Phys. Rev. B **92**, 054431 (2015), URL <https://link.aps.org/doi/10.1103/PhysRevB.92.054431>.
- ³⁴ C. Morari, W. H. Appelt, A. Östlin, A. Prinz-Zwicky, U. Schwingenschlögl, U. Eckern, and L. Chioncel, Phys. Rev. B **96**, 205137 (2017), URL <https://link.aps.org/doi/10.1103/PhysRevB.96.205137>.
- ³⁵ A. I. Lichtenstein and M. I. Katsnelson, Phys. Rev. B **57**, 6884 (1998), URL <https://link.aps.org/doi/10.1103/PhysRevB.57.6884>.
- ³⁶ M. I. Katsnelson and A. I. Lichtenstein, J. Phys.: Condens. Matter **11**, 1037 (1999).
- ³⁷ M. I. Katsnelson and A. I. Lichtenstein, Eur. Phys. J. B **30**, 9 (2002).
- ³⁸ L. V. Pourovskii, M. I. Katsnelson, and A. I. Lichtenstein, Phys. Rev. B **73**, 060506 (2006), URL <https://link.aps.org/doi/10.1103/PhysRevB.73.060506>.
- ³⁹ M. Jarrell and J. Gubernatis, Physics Reports **269**, 133 (1996), ISSN 0370-1573, URL <https://www.sciencedirect.com/science/article/pii/0370157395000747>.
- ⁴⁰ A. W. Sandvik, Phys. Rev. B **57**, 10287 (1998), URL <https://link.aps.org/doi/10.1103/PhysRevB.57.10287>.
- ⁴¹ K. S. D. Beach, R. J. Gooding, and F. Marsiglio, Phys. Rev. B **61**, 5147 (2000), URL <https://link.aps.org/doi/10.1103/PhysRevB.61.5147>.
- ⁴² D. Jacob, Journal of Physics: Condensed Matter **27**, 245606 (2015), URL <https://doi.org/10.1088/0953-8984/27/24/245606>.
- ⁴³ A. Droghetti and I. Rungger, Phys. Rev. B **95**, 085131 (2017), URL <https://link.aps.org/doi/10.1103/PhysRevB.95.085131>.
- ⁴⁴ I. Rungger, A. Droghetti, and M. Stamenova, in *Handbook of Materials Modeling. Vol. 1 Methods: Theory and Modeling*, edited by S. Yip and W. W. Andreoni (Springer International Publishing, 2019).
- ⁴⁵ Tréglia, G., Ducastelle, F., and Spanjaard, D., J. Phys. France **43**, 341 (1982), URL <https://doi.org/10.1051/jphys:01982004302034100>.
- ⁴⁶ A. A. Aligia, Phys. Rev. B **74**, 155125 (2006), URL <https://link.aps.org/doi/10.1103/PhysRevB.74.155125>.
- ⁴⁷ A. Kubetzka, M. Bode, O. Pietzsch, and R. Wiesendanger, Phys. Rev. Lett. **88**, 057201 (2002), URL <https://link.aps.org/doi/10.1103/PhysRevLett.88.057201>.
- ⁴⁸ S. Samarin, O. Artamonov, P. Guagliardo, K. Sudarshan, M. Kostylev, L. Pravica, A. Baraban, and J. Williams, Surface Science **617**, 22 (2013), ISSN 0039-6028, URL <https://www.sciencedirect.com/science/article/pii/S0039602813002185>.
- ⁴⁹ A. R. Rocha, V. M. García-Suárez, S. Bailey, C. Lambert, J. Ferrer, and S. Sanvito, Phys. Rev. B **73**, 085414 (2006), URL <https://link.aps.org/doi/10.1103/PhysRevB.73.085414>.
- ⁵⁰ A. Szabo and N. S. Ostlund, *Modern Quantum Chemistry: Introduction to Advanced Electronic Structure Theory* (Dover Publications Inc., Mineola NY, 1996).
- ⁵¹ J. M. Soler, E. Artacho, J. D. Gale, A. García, J. Junquera, P. Ordejón, and D. Sánchez-Portal, Journal of Physics: Condensed Matter **14**, 2745 (2002), URL <https://doi.org/10.1088/0953-8984/14/11/302>.
- ⁵² I. Rungger and S. Sanvito, Phys. Rev. B **78**, 035407 (2008), URL <https://link.aps.org/doi/10.1103/PhysRevB.78.035407>.
- ⁵³ D. Jacob, K. Haule, and G. Kotliar, Phys. Rev. Lett. **103**, 016803 (2009), URL <https://link.aps.org/doi/10.1103/PhysRevLett.103.016803>.
- ⁵⁴ D. Jacob and G. Kotliar, Phys. Rev. B **82**, 085423 (2010), URL <https://link.aps.org/doi/10.1103/PhysRevB.82.085423>.
- ⁵⁵ W. H. Appelt, A. Droghetti, L. Chioncel, M. M. Radonjić, E. Muñoz, S. Kirchner, D. Vollhardt, and I. Rungger, Nanoscale **10**, 17738 (2018), URL <http://dx.doi.org/10.1039/C8NR03991G>.
- ⁵⁶ E. Pavarini, in *The LDA+DMFT approach to strongly correlated materials Modeling and Simulation Vol. 1*, edited by E. Pavarini, E. Koch, D. Vollhardt, and A. Lichtenstein (Forschungszentrum Jülich, 2011).
- ⁵⁷ M. Karolak, G. Ulm, T. Wehling, V. Mazurenko, A. Poteryaev, and A. Lichtenstein, Journal of Electron Spectroscopy and Related Phenomena **181**, 11 (2010), ISSN 0368-2048, URL <https://www.sciencedirect.com/science/article/pii/S0368204810001222>.
- ⁵⁸ K. Haule, C.-H. Yee, and K. Kim, Phys. Rev. B **81**, 195107 (2010), URL <https://link.aps.org/doi/10.1103/PhysRevB.81.195107>.
- ⁵⁹ N. Bickers and D. Scalapino, Annals of Physics **193**, 206 (1989), ISSN 0003-4916, URL <https://www.sciencedirect.com/science/article/pii/000349168990359X>.
- ⁶⁰ G. Baym and L. P. Kadanoff, Phys. Rev. **124**, 287 (1961), URL <https://link.aps.org/doi/10.1103/PhysRev.124.287>.
- ⁶¹ G. Baym, Phys. Rev. **127**, 1391 (1962), URL <https://link.aps.org/doi/10.1103/PhysRev.127.1391>.
- ⁶² G. Stefanucci and R. van Leeuwen, *Nonequilibrium Many-Body Theory of Quantum Systems: A Modern Introduction* (Cambridge University Press, 2013).

- ⁶³ V. M. Galitski, Zh. Eksp. Teor. Fiz. **34**, 1011 (1958).
- ⁶⁴ J. Kanamori, Progress of Theoretical Physics **30**, 275 (1963), ISSN 0033-068X, <https://academic.oup.com/ptp/article-pdf/30/3/275/5278869/30-3-275.pdf>, URL <https://doi.org/10.1143/PTP.30.275>.
- ⁶⁵ J. W. Serene and D. W. Hess, Phys. Rev. B **44**, 3391 (1991), URL <https://link.aps.org/doi/10.1103/PhysRevB.44.3391>.
- ⁶⁶ A. Liebsch and A. Lichtenstein, Phys. Rev. Lett. **84**, 1591 (2000), URL <https://link.aps.org/doi/10.1103/PhysRevLett.84.1591>.
- ⁶⁷ B. Himmetoglu, A. Floris, S. de Gironcoli, and M. Cococcioni, International Journal of Quantum Chemistry **114**, 14 (2014), <https://onlinelibrary.wiley.com/doi/pdf/10.1002/qua.24521>, URL <https://onlinelibrary.wiley.com/doi/abs/10.1002/qua.24521>.
- ⁶⁸ M. T. Czyżyk and G. A. Sawatzky, Phys. Rev. B **49**, 14211 (1994), URL <https://link.aps.org/doi/10.1103/PhysRevB.49.14211>.
- ⁶⁹ V. I. Anisimov and O. Gunnarsson, Phys. Rev. B **43**, 7570 (1991), URL <https://link.aps.org/doi/10.1103/PhysRevB.43.7570>.
- ⁷⁰ T. Andersen and W. Hübner, Phys. Rev. B **74**, 184415 (2006), URL <https://link.aps.org/doi/10.1103/PhysRevB.74.184415>.
- ⁷¹ K. Zakeri, Y. Zhang, J. Prokop, T.-H. Chuang, N. Sakr, W. X. Tang, and J. Kirschner, Phys. Rev. Lett. **104**, 137203 (2010), URL <https://link.aps.org/doi/10.1103/PhysRevLett.104.137203>.
- ⁷² O. Gunnarsson, Journal of Applied Physics **49**, 1399 (1978), <https://doi.org/10.1063/1.325005>, URL <https://doi.org/10.1063/1.325005>.
- ⁷³ R. Zeller, in *Magnetism, in Computational Nanoscience: Do It Yourself!*, edited by J. Grotendorst, S. Blügel, and D. Marx (NIC Serie, Forschungszentrum Jülich, 2006), <http://juser.fz-juelich.de/record/54009/files/FZJ-2014-02225.pdf>.
- ⁷⁴ J. Brede, N. Atodiresei, S. Kuck, P. Lazić, V. Caciuc, Y. Morikawa, G. Hoffmann, S. Blügel, and R. Wiesendanger, Phys. Rev. Lett. **105**, 047204 (2010), URL <https://link.aps.org/doi/10.1103/PhysRevLett.105.047204>.